nature chemical biology

ARTICLES

https://doi.org/10.1038/s41589-018-0009-4

Resistance to nonribosomal peptide antibiotics mediated by D-stereospecific peptidases

Yong-Xin Li[1,2], Zheng Zhong[1], Peng Hou[1], Wei-Peng Zhang[1] and Pei-Yuan Qian[1]*

Nonribosomal peptide antibiotics, including polymyxin, vancomycin, and teixobactin, most of which contain D-amino acids, are highly effective against multidrug-resistant bacteria. However, overusing antibiotics while ignoring the risk of resistance arising has inexorably led to widespread emergence of resistant bacteria. Therefore, elucidation of the emerging mechanisms of resistance to nonribosomal peptide antibiotics is critical to their implementation. Here we describe a networking-associated genome-mining platform for linking biosynthetic building blocks to resistance components associated with biosynthetic gene clusters. By applying this approach to 5,585 complete bacterial genomes spanning the entire domain of bacteria, with subsequent chemical and enzymatic analyses, we demonstrate a mechanism of resistance toward nonribosomal peptide antibiotics that is based on hydrolytic cleavage by D-stereospecific peptidases. Our finding reveals both the widespread distribution and broad-spectrum resistance potential of D-stereospecific peptidases, providing a potential early indicator of antibiotic resistance to nonribosomal peptide antibiotics.

The emergence of antibiotic resistance coupled with the scarcity of new antibiotics is causing a global health crisis in the twenty-first century[1]. Nonribosomal peptides (NRPs), which are biosynthesized by large, modular, multifunctional enzymes known as nonribosomal peptide synthetases (NRPSs), are among the most widespread and structurally diverse antibiotics in nature. In addition to proteinogenic amino acids, NRPSs can also incorporate nonproteinogenic amino acids, such as D-amino acids (D-aa), dramatically expanding their bioactive chemical space[2–6]. The increasing problem of bacterial resistance to many current antibiotics has led to rising interest in the therapeutic potential of NRP antibiotics[3]. Current peptide antibiotic drugs, such as bacitracin, daptomycin, polymyxin, and vancomycin, most of which are D-aa-containing NRP (DNRP) antibiotics, constitute very effective treatments for infections caused by drug-resistant pathogens[2–4]. However, overuse of these antibiotics over decades has inexorably resulted in the widespread emergence of resistant bacteria[7,8]. Current resistance mechanisms to these peptide antibiotics mainly involve modifying bacterial cell walls or membranes and reducing drug binding affinity[7–9]. For instance, resistance to the DNRP vancomycin is developed when DD-peptidases VanX and VanY catalyze the removal of the drug's target in peptidoglycans of Gram-positive bacteria, thus reducing the binding affinity of vancomycin[10]. DNRPs that overcome established clinical resistance mechanisms, including ramoplanin, tridecaptin, lugdunin, and teixobactin, have been introduced as attractive therapeutic candidates[4,11–13]. However, as they possess a remarkable ability to rapidly adapt in response to antibiotics, bacteria will eventually evolve to harbor resistance to new antibiotics. These inevitable cycles of antibiotic discovery and resistance not only present the risk of overconfidence in peptide antibiotics, but also highlight the importance of elucidating emerging resistance mechanisms[9].

Antibiotic producers harbor intrinsic resistance determinants that typically function with a specific class of small molecules for self-protection and are often associated with antibiotic biosynthetic gene clusters (BGCs). BGCs constitute a source of emerging resistance that might possess clinical relevance[14–16]. In the present report, we describe a networking-associated global genome-mining approach that links the chemical building blocks of DNRPs to resistance genes associated with their BGCs. By applying this approach to publicly available complete bacterial genomes, we identified a family of D-stereospecific peptidases that are phylogenetically widely distributed in nature. This mechanism of D-stereospecific resistance that was identified by global genome mining was experimentally validated by a combination of chemical and enzymatic analyses. Additionally, these D-stereospecific resistance peptidases possess broad-spectrum resistance against current and new antibiotics, demonstrating their potential to pose a risk to human health if transferred to pathogens.

RESULTS

Linking D-aa to resistance elements by networking. Current genome-mining strategies rely heavily on comparing sequences with known BGCs to identify uncharacterized BGCs[17,18], limiting the potential linking of chemistry with biology. Here we developed a global genome-mining platform that targets the specific underlying biosynthetic logic of BGCs in 5,585 complete bacterial genomes available online by parsing the pattern depending on the presence or absence of biosynthesis elements, such as assembling and tailoring domains and proteins (Supplementary Fig. 1). Our global analysis of 6,879 NRPS BGCs through the application of this approach revealed 2,511 BGCs encoding DNRPs (36.5%) that are extremely diverse and widely distributed throughout the bacterial domain (Supplementary Figs. 2 and 3). In addition, the majority of these BGCs are uncharacterized and have the potential for novel natural product production.

We next sought to determine the hidden biosynthetic logic linking the D-aa building blocks of DNRPs and their associated enzymes, transporters, and regulators by using global co-occurrence-network-based analysis of biosynthetic elements in pattern matrices, with the ultimate goal of identifying a set of resistance determinants that recognize and function specifically with DNRPs. The resulting

[1]Department of Ocean Science and Division of Life Science, Hong Kong University of Science and Technology, Clear Water Bay, Hong Kong, China. [2]Institute for Advanced Study, Hong Kong University of Science and Technology, Clear Water Bay, Hong Kong, China. *e-mail: boqianpy@ust.hk

co-occurrence network revealed an unexpected finding: there are specific sets of BGC-associated resistance elements that are significantly associated with the D-aa building blocks of DNRPs (Fisher's exact test; $P_1 < 0.005$, $P_2 < 0.05$; Fig. 1a and Supplementary Fig. 4). D-Leu, D-Cys, and D-Glu were found to be frequent drivers of network connections with transporters and regulators, whereas D-Thr, D-ornithine (D-Orn), and D-Ser were mainly associated with enzymes, likely because D-aa that have hydroxyl and amine groups tended to be enzymatically modified by tailoring enzymes such as acyltransferases or glycosyltransferases.

Remarkably, the BGC-associated peptidases (E5), which are a cluster of the orthologous group of MEROPS S12 peptidases collected on the basis of seed alignment in AntiSMASH[19], were connected to a range of different DNRPs. The two best-known representatives of MEROPS S12 peptidases are DD-carboxypeptidase and β-lactamase. The former is involved in the synthesis and remodeling of bacterial cell walls, whereas the latter is well known to confer resistance to β-lactam family antibiotics[9,10,20,21]. Global analysis of 26,344 bacterial BGCs detected 1,282 E5 enzymes, which are phylogenetically widely distributed in bacteria. Moreover, 218 (8.7%) DNRP BGCs harbored a BGC-associated E5. Although classic β-lactamases in pathogens are well known to confer resistance to β-lactam-family antibiotics, the function of putative β-lactamases in native microbial communities remains poorly understood[20,21]. The strong association between E5 and the total D-aa exhibited in Firmicutes (Fig. 1b) and the associations (6- to 12-fold above average) between E5 and individual D-aa blocks observed at the genus level (Fig. 1c) further suggest that the widely distributed DNRP BGC-associated E5s may be D-stereospecific peptidases that function specifically with DNRPs. In particular, the extremely strong association (of the 73 BGCs that encode D-Asn1-containing NRPs, 72 of them harbor E5; $P_1 = 4.1 \times 10^{-83}$) between E5 and a D-Asn1 building block corroborates recent findings of a widespread D-Asn1-specific activation mechanism of the *N*-acyl-D-Asn1 precursor[22–24]. In contrast to D-Asn1 activation peptidases, which are conserved across the bacterial domain, other peptidases correlated

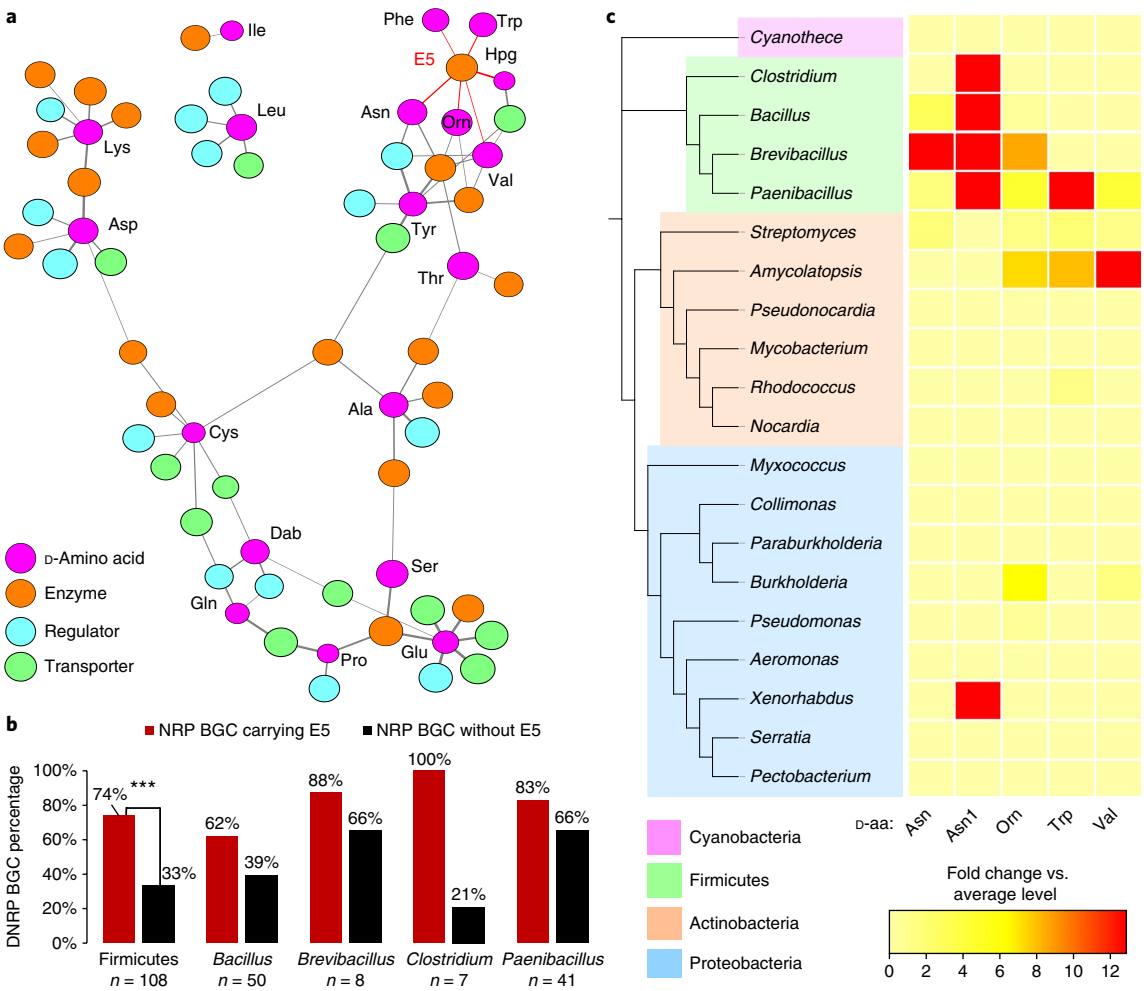

Fig. 1 | Co-occurrence networks reveal the widespread distribution of BGC-associated D-stereospecific peptidases. a, Pairwise co-occurrence network between D-amino acid (D-aa) and resistance elements (enzymes, regulators, and transporters). Major lineages between D-aa of DNRPs and their BGC-associated resistance elements were extracted from the co-occurrence network (Supplementary Fig. 4). The thickness of each connection (edge) represents the relative proportion of D-aa associated with antibiotic determinants, and the size of each node represents the relative abundance of each biosynthesis element. Only BGC-associated enzymes discussed within this study are labeled. **b**, Relative proportion of DNRP BGCs in NRP BGCs with or without E5 in Firmicutes and its four genera (n = the number of NRP BGCs carrying E5). The result indicates a strong association of E5 with DNRP BGCs in Firmicutes (P values were determined using the two-sided Fisher's exact test; $^{***}P < 0.001$). **c**, Heat map of the association between D-aa of DNRPs ($n \geq 3$) and E5 at the genus level. Colors in the heat map represent fold change of the proportion of DNRP BGCs carrying E5 in DNRP BGCs against the proportion of NRP BGCs carrying E5 in NRP BGCs.

with D-aa were divergent and diverse (Supplementary Figs. 5–8). Taking into consideration the substantial differences in the putative D-aa arrangement patterns in DNRPs (Supplementary Figs. 9 and 10), we predicted that the other D-aa-correlated peptidases might be involved in D-stereospecific self-resistance of DNRPs rather than pro-drug activation. We therefore designated these peptidases as D-stereospecific resistance peptidases (DRPs).

Biosynthetic and metabolic analysis of DNRPs. As the most extensive association was observed in Firmicutes (Fig. 1b,c), we focused our follow-up screening on NRPs with potential D-stereospecific self-resistance enzymes in the genera *Brevibacillus* and *Paenibacillus*. To evaluate whether the putative DRPs possess D-stereospecific cleavage activity, we selected putative DRP genes *triF* and *bogQ* (associated with tridecaptin and bogorol BGCs, respectively; Fig. 2a and Supplementary Figs. 9 and 10) for further investigation. *Brevibacillus laterosporus* DSM 25 and ATCC 9141, which harbor an active bogorol gene cluster (*bogA–Q*), and *Paenibacillus polymyxa* CICC10580, which harbors active tridecaptin gene clusters (*triA–F* and *trbA*), were selected on the basis of genome-mining and metabolic analysis (Fig. 2). Both of these strains produced corresponding truncated products that were cleaved from bactericidal DNRPs, as established by MS/MS and NMR analyses of peptides isolated from fermentation broths[12,25–28] (Supplementary Note). We predicted that truncated products were generated from parent tridecaptins (**1** and **2**) or bogorols (**3**–**8**) by cleaving the central amide bond at specific D-aa carbonyl groups. Compounds **9**–**12** were D-Orn4 and D-Lys8 hydrolytic products of bogorol A (**3**), whereas compounds **13** and **14** were D-Trp5 hydrolytic products of tridecaptin B (**1**) (Fig. 2b–d and Supplementary Fig. 11). These hydrolytic products (**9**–**11**, **13**, and **14**) lacked antibacterial activity at concentrations of 128 μg mL^{-1} (Supplementary Table 1), indicating that BogQ and TriF might be peptidases for antibiotic self-resistance.

The predicted biosynthesis of bogorol starts with two NRPS modules that introduce 2-hydroxy-3-methylpentanoic acid (Hmp), a carboxylic acid, and dehydroamino acid (Aba), a noncanonical amino acid. In accordance with the co-linearity rule, the other 12 amino acids, including DRP-recognition residues D-Orn4 and D-Lys8, are introduced into the linear peptide, and the final product alcohol, bogorol, is reductively released by the reductase domain of BogF (Supplementary Fig. 10). Taken together, we anticipated that the D-Orn4- and D-Lys8-'labeled' antibiotic bogorols would be produced by their host to inhibit their competitors, and the putative DRP would be employed as an inactivation enzyme to modify antibiotics for self-protection. A similar self-protection strategy was also employed in the tridecaptin biosynthesis pathway (Supplementary Table 1 and Supplementary Fig. 12).

Biochemical characterization of DRPs BogQ and TriF. BogQ is a putative S-layer-associated protein, whereas TriF is a putative membrane-associated protein, and both of these harbor a signal sequence and a MEROPS S12 peptidase catalytic domain based on in silico analysis[29,30]. To evaluate whether DRPs BogQ and TriF are capable of cleaving DNRPs, we cloned the genes and expressed

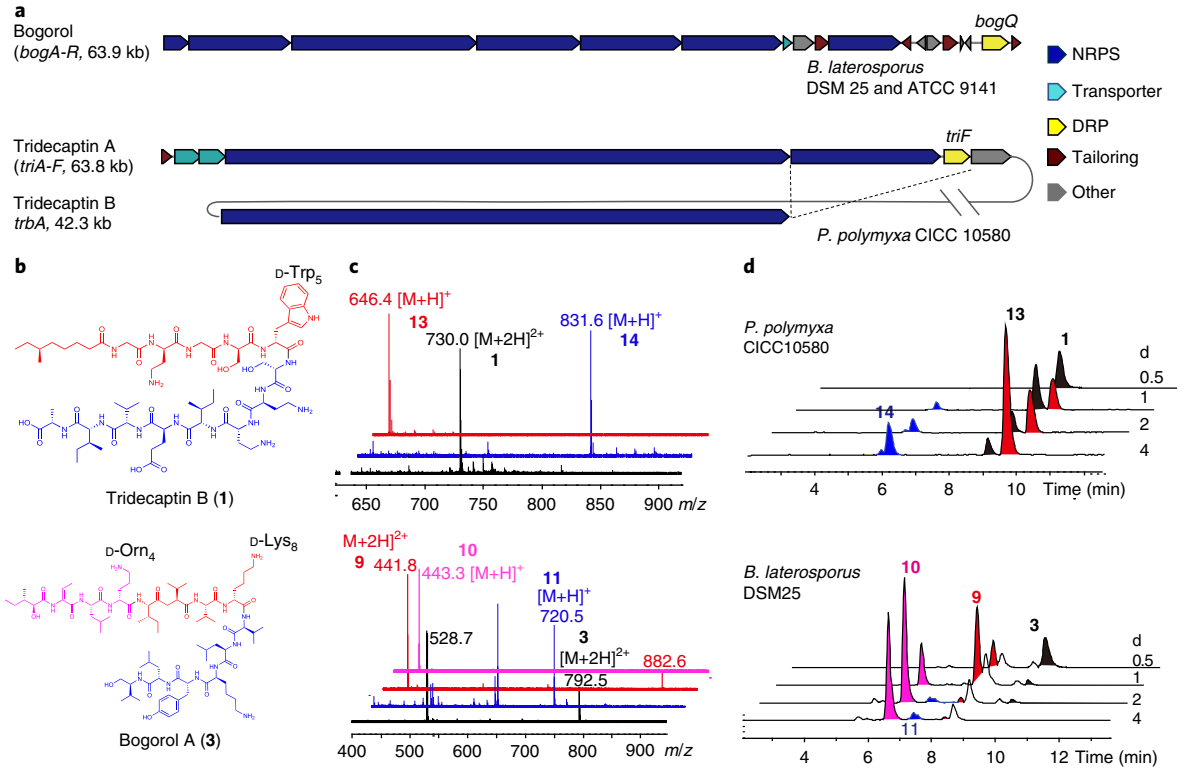

Fig. 2 | Genetic and metabolic analyses reveal the D-stereospecific hydrolytic activities of DRPs. a, The BGCs of bogorol from *B. laterosporus* DSM 25 and ATCC 9141, as well as tridecaptin A and tridecaptin B from *P. polymyxa* CICC 10580. BogQ from the strain DSM 25 and that from the strain ATCC 9141 share 85% amino acid sequence identity. The intersecting dotted lines indicate genes shared by two gene clusters within the same host (Supplementary Fig. 10). **b**, Structures of DNRPs tridecaptin B and bogorol A, with DRP recognition motifs highlighted. **c**, Stacked overlay of the mass spectra (electrospray ionization) of parent compounds (black), C-terminal fragments (blue), and N-terminal fragments (red). Data are representative of two independent experiments. Top, tridecaptin B; bottom, bogorol A. **d**, Time-course analyses of corresponding compounds produced by *P. polymyxa* CICC 10580 (top) and *B. laterosporus* DSM 25 (bottom) at different fermentation times (representative of three independent experiments). For enzymatic cleavage patterns, see Supplementary Fig. 11.

the enzymes for in vitro characterization (Supplementary Fig. 13). The soluble periplasmic peptidase domain of TriF ($TriF_{pep}$) without the signal peptide or four hydrophobic C-terminal transmembrane helices was overexpressed and purified. TriF and BogQ exhibited D-stereospecific hydrolysis activity against their correlated DNRPs in an in vitro assay (Fig. 3a–c). According to comparisons of the primary structures, the peptidase domain exhibits two conserved motifs (SxxK and Yxx) that characterize the catalytic center of the MEROPS S12 enzyme family[29]. The hydrolytic activity of BogQ mutants (S106A or Y200A) and TriF mutants (S95A or Y190A) was completely abolished, confirming that their activity is caused by the peptidase catalytic domain. TriF exhibited specific amide bond hydrolytic activity at the C-terminal side of D-Trp in both **1** and oct-tridecaptin A (**22**; Fig. 3b,c), whereas BogQ strongly targeted the C-terminal sides of D-Orn and D-Lys in **3** (Fig. 3a) as expected.

The strong preference for D-Orn4 and D-Lys8 compared to L-Lys11 in the bogorols (**3**–**8**; Supplementary Table 2) indicated the D-stereospecific selectivity of BogQ, which was further supported by the preference of BogQ for D-diaminobutyric acid (Dab)2 and D-Dab8 over the L-Dab7 of exogenous tridecaptin (**1**; Fig. 3b). To ascertain the D-stereospecific selectivity of BogQ and TriF, we assayed a series of tridecaptin and bogorol derivatives (**22**–**36** and **37**–**44**, respectively) with varying recognition motifs (Supplementary Table 2). As anticipated, C- and N-terminal hydrolytic fragments corresponding to the L enantiomer motifs were not detected in BogQ assays against L-Orn-truncated bogorols (**39** and **43**) or L-Dab2 and L-Dab8 tridecaptins (**23** and **24**) or in $TriF_{pep}$ assays against an L-Trp5 tridecaptin derivative (**25**; Supplementary Table 2). Comparison of the cleavage efficiencies of BogQ against D- or L-Orn-bogorol derivatives (Fig. 3d, **38** vs. **39** and **42** vs. **43**), BogQ against D- or L-Trp-tridecaptins (Fig. 3e, **22** vs. **23** and **24**), and $TriF_{pep}$ against D- or L-Trp-tridecaptins (Figs. 3f, 1 and **22** vs. **25**) further verified their D-stereospecific selectivity.

Notably, both endogenous bogorols and exogenous tridecaptins were specifically hydrolyzed by BogQ at the site of positively charged D-Lys, D-Orn or D-Dab, implying that BogQ has broad substrate tolerance against cationic antibiotics. Comparison of the cleavage efficiency of BogQ against **28**–**36** and **37**–**44** not only confirmed its D-stereospecific selectivity but also revealed its broad range of recognition motifs (positively charged D-aa Lys, Orn, Dab, and Arg; Supplementary Table 2). Additionally, synthetic and natural peptides ranging from 2 aa to 13 aa were D-stereospecifically hydrolyzed by their corresponding DRPs and showed various cleavage efficiencies regardless of dynamic variations in the substrate residues S2 and S1' (Supplementary Table 2). Our results suggest that the corresponding D-aa are the minimal recognition motifs; i.e., positively charged D-aa for BogQ and D-Trp for TriF. The minimal recognition motifs not only ensure the selectivity of D-aa but also enlarge their potential resistance spectra.

Intriguingly, the complete abolishment of BogQ hydrolytic activity against tri-Boc-protected bogorol (**45**; Fig. 3g) and the dramatic decrease in hydrolytic activity against Gln2-substituted **38** (Fig. 3h, **37** vs. **38**) revealed that a positively charged side chain is crucial for BogQ cleavage efficiencies. This positively charged feature of DNRPs may facilitate electrostatic interactions with BogQ, which has a negatively charged substrate-binding pocket, as predicted by homology modeling (Supplementary Figs. 14 and 15). This implication was further supported by comparing cleavage efficiencies of peptides with various charges (Fig. 3g). The S-layer homology (SLH) domains of the putative S-layer-associated

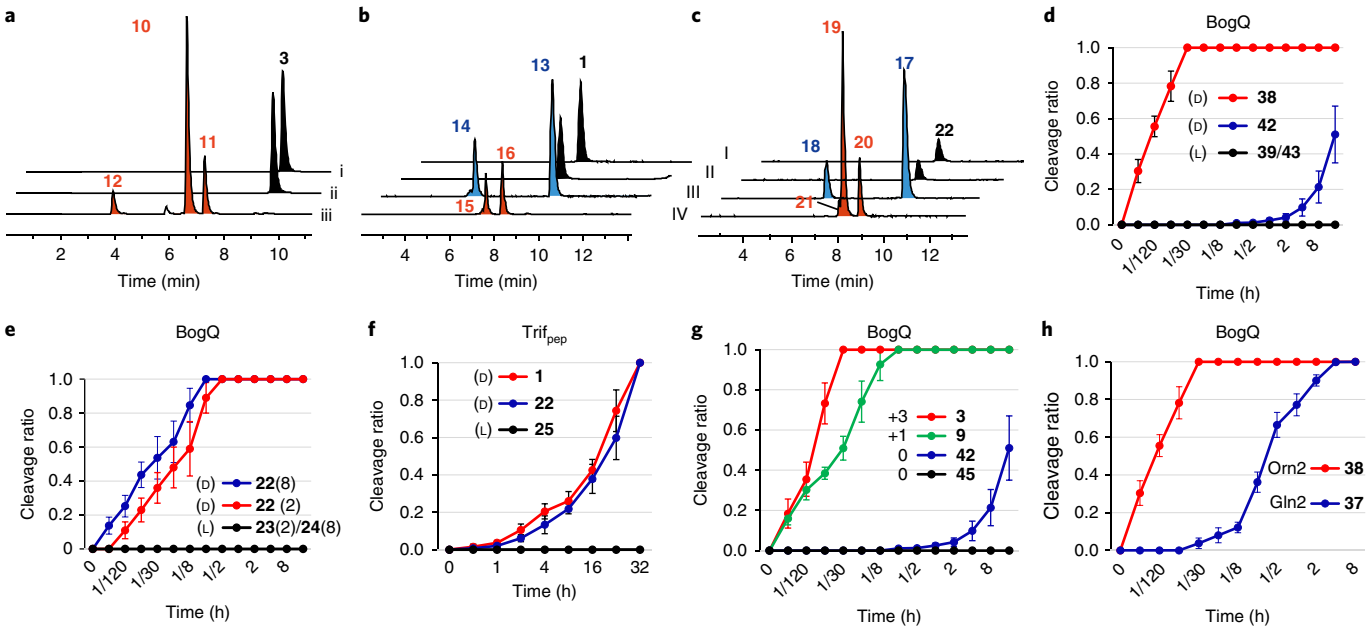

Fig. 3 | In vitro characterization reveals the D-stereospecific hydrolytic activities of DRPs. a–**c**, LC–MS traces of in vitro assays of BogQ, $TriF_{pep}$, and variants (2.0 μM) with bogorol A (**a**), tridecaptin B (**b**), and oct-tridecaptin A (**c**). Data are representative of three independent experiments. For **a**, (i) substrate standard (**3**, 200 μM), (ii) incubation of the substrate with the BogQ mutant (S106A) for 1 h, and (iii) incubation of the substrate with BogQ for 1 h; for **b**,**c**, (i) substrate standard (**1** or **22**, respectively, 20 μM), (ii) incubation of the substrate with the $TriF_{pep}$ mutant (S95A) for 24 h, (iii) incubation of the substrate with $TriF_{pep}$ for 24 h, and (iv) incubation of the substrate with BogQ for 1 h. **d**, Time-course in vitro study of BogQ (2.0 μM) against D- and L-Orn bogorol analogs (**38** vs. **39** and **42** vs. **43**; 200 μM; D/L-configurations of cleavage sites are indicated). **e**, Time-course in vitro study of BogQ (2.0 μM) against D- and L-Dab tridecaptins (**22**–**24**, 200 μM). The cleavage efficiency at the Dab2 site (2) in **22** vs. **23** and that at the Dab8 site (8) in **22** vs. **24** are shown for comparison. **f**, Time-course in vitro study of $TriF_{pep}$ (2.0 μM) against D- and L-Trp tridecaptins (**1** and **22** vs. **25**, 200 μM). **g**, Time-course in vitro assay of BogQ (2.0 μM) against bogorol analogs (**3**, **9**, **42**, and **45**; 200 μM) with various net charges (0, +1, +3). **h**, Time-course in vitro assay of BogQ (2.0 μM) against bogorol analog **38** and its D-Gln2-substituted analog (**37**; 200 μM). For **d**–**h**, data are mean ± s.d.; $n = 3$ independent experiments.

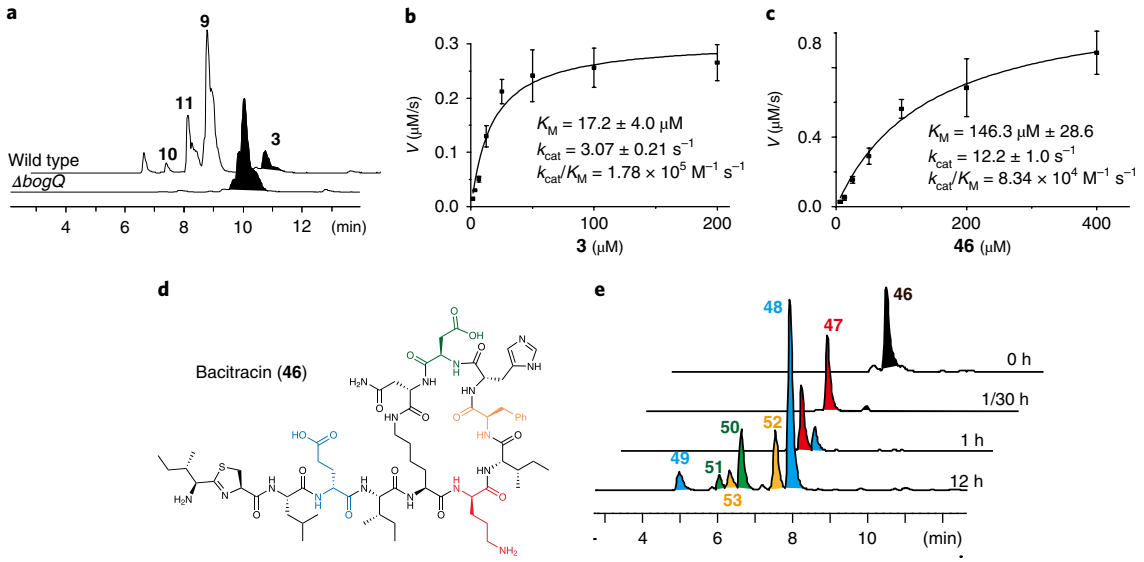

Fig. 4 | Biochemical analyses reveal the broad-spectrum resistance of BogQ against peptide antibiotics. a, LC–MS traces comparing wild-type *B. laterosporus* ATCC 9141 and the Δ*bogQ* mutant (representative of three independent experiments). **b**,**c**, Kinetic analyses of BogQ-catalyzed hydrolysis of bogorol A (**b**; **3**) and bacitracin (**c**; **46**) *v*, reaction velocit. Data are mean ± s.d.; $n = 3$ independent experiments. **d**, Structure of the DNRP antibiotic bacitracin; colors highlight the cleavage sites of BogQ. **e**, LC–MS traces of in vitro assays of BogQ (2.0 μM) against **46** (200 μM; representative of two independent experiments). Time-course cleavage products (**47**–**53**) of **46** are labeled using the same color code as their D-aa cleavage sites in **d**. For enzymatic cleavage patterns, see Supplementary Fig. 22.

BogQ are rich in negatively charged residues, with an isoelectric point of ~5, and may also promote favorable electrostatic interactions with cationic peptides. The enzymatic activity of $BogQ_{pep}$ without the negatively charged SLH domains is decreased dramatically compared to that of BogQ (Supplementary Table 2). Taken together, these results suggest that BogQ potentially targets peptides containing cationic D-aa, which is 31.1% of bacterial DNRPs (782/2,511).

The impact of DRPs in antibiotic resistance. To evaluate whether putative DRPs are involved in the self-resistance of DNRP antibiotics, we attempted to generate Δ*bogQ* or Δ*triF* mutant strains of *B. laterosporus* ATCC 9141 and DSM 25 or *P. polymyxa* CICC10580. However, only a mutant strain of *B. laterosporus* ATCC 9141 was successfully generated using the CRISPR–Cas9 gene-editing system[31,32] (Supplementary Fig. 16) after numerous attempts. No hydrolytic fragment corresponding to bogorol was detected in the Δ*bogQ* mutant strain, further supporting the in vivo function of BogQ (Fig. 4a). The minimum inhibitory concentration (MIC) was determined to establish whether the Δ*bogQ* mutant presented increased susceptibility or resistance to bogorols (Table 1). The Δ*bogQ* mutant was more susceptible (eight-fold) to bogorols than the wild-type strain, but it was not susceptible to kanamycin.

We next evaluated the catalytic efficiency of BogQ by determining its enzyme kinetics to further verify whether the BogQ hydrolysis of DNRPs was physiologically relevant to its self-resistance. In agreement with the high MIC value of **3** against *B. laterosporus* expressing BogQ (Table 1) the enzyme had high catalytic efficiency ($k_{cat}/K_M = 1.78 \times 10^5\ M^{-1}\ s^{-1}$) against **3** (Fig. 4b). S-layer protein, which may function as a protection barrier for cationic peptide antibiotics through electrostatic interaction, has been reported to confer resistance against cationic antimicrobial peptides[30]. Together, our results indicate that the putative S-layer-associated protein BogQ, with hydrolytic activity, functions as a self-protective barrier against antibiotic bogorols (Supplementary Fig. 12). However, the possible role of BogQ and other putative DRPs in bacterial peptidoglycan remodeling remains to be elucidated.

Given the potential of BogQ for broad-spectrum resistance, we investigated the presence of BogQ-like peptidases aside from the putative D-Orn-correlating BGC-associated peptidases. In total, we identified 403 putative peptidases with similar domain compositions from publicly available bacterial genomes,

Table 1 | Antibiotic resistance of *Brevibacillus laterosporus* with BogQ against peptide antibiotics

	MIC (μg/mL)					
Strain and genotype	**Bs**	**3**	**46**	**Enduracidin**	**Ramoplanin**	**Kanamycin**
B. laterosporus DSM 25	512	512	2,048	4	4	16
B. laterosporus ATCC 9141 (WT)	512	512	2,048	4	4	8
B. laterosporus ATCC 9141(Δ*bogQ*)	64	64	512	4	4	8
B. subtilis 168	16	4	256	0.25	0.5	–
S. aureus ATCC 43300	16	8	64	1	2	–

MIC was determined by broth microdilution. Bs, total bogorols extracted from *B. laterosporus* ATCC 9141.

consisting of a S12 peptidase domain and two or three SLH domains in the carboxy-terminal region, most of which are harbored by the genera *Bacillus*, *Brevibacillus*, and *Paenibacillus* of the Bacillales order. The strong association (Mann–Whitney U test) of BogQ-like peptidase with NRP BGCs, especially DNRP BGCs at the genome level, suggests that the widely distributed BogQ-like peptidases in the Bacillales order may be involved in resistance to NRP antibiotics (Supplementary Fig. 17).

We next determined the potential impact of BogQ on D-aa-containing peptide antibiotics. Inhibitors of bacterial cell wall biosynthesis, including bacitracin, polymyxin, teixobactin, enduracidin, ramoplanin, mannopeptimycin, hypeptin, and katanosin B, have already been intensively studied because the risk of resistance emerging from them is low[11,12,33,34]. Daptomycin, A54145, and lysocin E, which target the bacterial cell membrane, constitute other antibiotics that are ideal for treating infections caused by drug-resistant pathogens, as resistance acquisition also seems challenging for bacteria[34]. Most of these antibiotics possess a certain structural archetype in which they carry positively charged D-aa (Lys, Orn, Dab, Arg, and guanidine amino acids; Supplementary Fig. 18). Current resistance to these antibiotics is often associated with changes in the expression of regulators, which results in modification of cell walls or membranes and reduction of inhibitor binding[9]. In addition to preventing antibiotics from accessing targets or altering their targets, bacteria can inactivate antibiotics using modification enzymes.

Although the positively charged residues may play an essential role in the interaction with cell wall precursors or cell membranes, they may also offer unique targets for inactivation enzymes, such as BogQ. Indeed, BogQ exhibited enzymatic inactivation against these selected peptide antibiotics containing cationic D-aa, showing especially high catalytic efficiency against bacitracin (**46**) ($k_{cat}/K_M = 8.34 \times 10^4\,M^{-1}s^{-1}$; Fig. 4c–e and Supplementary Figs. 19–23). *B. laterosporus* expressing BogQ had MICs that were 2–128 times higher than those of *Bacillus subtilis* or *Staphylococcus aureus* for selected DRP antibiotics, whereas the Δ*bogQ* mutant was four times more susceptible to bacitracin than the wild-type *B. laterosporus* (Table 1). The results support the view that BogQ acts as a broad-spectrum resistance determinant for cationic D-aa-containing peptide antibiotics. Notably, as it exhibits D-stereospecific cleavage activities at the site of other uncharged or negatively charged D-amino acids (Gln, Glu, Asp, and Thr), BogQ may possess a broader resistance spectrum than we originally expected. Low cleavage activity with daptomycin and truncated teixobactin were also observed (Supplementary Fig. 23).

An important question yet to be answered is whether or not these DRPs are transferable. Putative DRP resistance determinants were found in the chromosome, and there is no evidence of flanking mobile elements. However, their relation (25.1%) with BGC-associated transposases, which were reported to be involved in the horizontal transfer of entire BGCs[35], suggests that mobilization is possible. Although the levels of resistance emerging from the hydrolytic activities of DRP (Supplementary Fig. 24) in host *Escherichia coli* and *B. subtilis* were low (one- to two-fold changes in MIC), the acquisition of DRPs could be advantageous for bacterial adaptation in environmental niches surrounded by DNRP antibiotic-producing organisms in which a gradient of antibiotic concentrations exists. The low resistance level could result from a number of factors, including enzyme expression level, transportation, and the locations of D-stereospecific resistance peptidases and binding targets of antibiotics. Taking into account their widespread distribution in the environment and their functionality in heterologous hosts, we envision that DRP resistance elements could eventually make their way into pathogens under selective pressure either with assistance from the BGC-associated transposases or in combination with mobile elements.

DISCUSSION

Our networking-associated global genome-mining approach not only enables the uncovering of the bacterial biosynthesis capacity of natural products, but also provides insight into their hidden biosynthetic logic. Applying this approach to complete bacterial genomes available online, we demonstrated that the genes for putative DRPs clustered with BGCs were widely distributed in bacteria. Additionally, by integrating a series of biosynthetic, chemical, and enzymatic analyses, we demonstrated the D-stereospecific selectivity of DRPs and their broad-spectrum potential. Given this uniqueness and the broad target spectrum, future work is envisaged to obtain atomistic structure information to elucidate the mechanism of peptide resistance. In addition to BGC-associated DRPs, microorganisms are known to express diverse D-stereospecific peptidases that are not associated with BGCs[20], and their role in antibiotics resistance may have been overlooked because of scant information available about their targets. The D-stereospecific enzymes screened from nature—β-lactamases, D-aminopeptidases, alkaline D-peptidases, and DD-carboxypeptidases—possess the common feature of using synthetic peptides containing D-aa. However, little is known about the function of the D-stereospecific peptidases, besides cell wall assemblage or β-lactam antibiotic resistance in the native microbial community[20]. DRP BogQ, a family of surface proteins from the MEROPS S12 peptidase, represents a new class of antibiotic resistance enzymes effective against peptide antibiotics via D-stereospecific cleavage of antibiotics. On the basis of our findings, we can hypothesize that the D-stereospecific enzyme family may be involved in combating widely distributed antibiotics containing D-aa for the survival of their host. We believe that finding DRPs in nature constitutes only the tip of the iceberg, which will lead to research on the use and development of peptide antibiotics to combat antibiotic resistance.

DNRPs that are widely distributed in bacteria represent a valuable source of antibiotics. Yet, little is known about the function of D-aa building blocks other than they provide architectural diversity of bioactive small molecules[5,6]. Our data showed that D-aa may also be employed by bacteria to label DNRP antibiotics for D-stereospecific self-resistance. Given the potential of DRPs for broad-spectrum antibiotic resistance and their ability to target clinically important antibiotics containing D-aa, these widely distributed resistance genes are likely to be particularly dangerous if they are transferred to opportunistic pathogens. Our findings not only warn against becoming overconfident in the power of extant and new peptide antibiotics, but also offer guidance to pharmaceutical chemists seeking to increase our collective antibiotic arsenal.

Methods

Methods, including statements of data availability and any associated accession codes and references, are available at https://doi.org/10.1038/s41589-018-0009-4.

Received: 27 September 2017; Accepted: 27 December 2017;
Published online: 26 February 2018

References

1. Laxminarayan, R. et al. Antibiotic resistance—the need for global solutions. *Lancet Infect. Dis.* **13**, 1057–1098 (2013).
2. Schwarzer, D., Finking, R. & Marahiel, M. A. Nonribosomal peptides: from genes to products. *Nat. Prod. Rep.* **20**, 275–287 (2003).
3. Hancock, R. E. W. & Chapple, D. S. Peptide antibiotics. *Antimicrob. Agents Chemother.* **43**, 1317–1323 (1999).
4. Law, V. et al. DrugBank 4.0: shedding new light on drug metabolism. *Nucleic Acids Res.* **42**, D1091–D1097 (2014).
5. Balibar, C. J., Vaillancourt, F. H. & Walsh, C. T. Generation of D amino acid residues in assembly of arthrofactin by dual condensation/epimerization domains. *Chem. Biol.* **12**, 1189–1200 (2005).
6. Cava, F., Lam, H., de Pedro, M. A. & Waldor, M. K. Emerging knowledge of regulatory roles of D-amino acids in bacteria. *Cell. Mol. Life Sci.* **68**, 817–831 (2011).

7. Liu, Y. Y. et al. Emergence of plasmid-mediated colistin resistance mechanism MCR-1 in animals and human beings in China: a microbiological and molecular biological study. *Lancet Infect. Dis.* **16**, 161–168 (2016).
8. Smith, T. L. et al. Emergence of vancomycin resistance in *Staphylococcus aureus*. *N. Engl. J. Med.* **340**, 493–501 (1999).
9. Blair, J. M. A., Webber, M. A., Baylay, A. J., Ogbolu, D. O. & Piddock, L. J. V. Molecular mechanisms of antibiotic resistance. *Nat. Rev. Microbiol.* **13**, 42–51 (2015).
10. Meziane-Cherif, D., Stogios, P. J., Evdokimova, E., Savchenko, A. & Courvalin, P. Structural basis for the evolution of vancomycin resistance D,D-peptidases. *Proc. Natl. Acad. Sci. USA* **111**, 5872–5877 (2014).
11. Ling, L. L. et al. A new antibiotic kills pathogens without detectable resistance. *Nature* **517**, 455–459 (2015).
12. Cochrane, S. A. et al. Antimicrobial lipopeptide tridecaptin A1 selectively binds to Gram-negative lipid II. *Proc. Natl. Acad. Sci. USA* **113**, 11561–11566 (2016).
13. Zipperer, A. et al. Human commensals producing a novel antibiotic impair pathogen colonization. *Nature* **535**, 511–516 (2016).
14. Thaker, M. N. et al. Identifying producers of antibacterial compounds by screening for antibiotic resistance. *Nat. Biotechnol.* **31**, 922–927 (2013).
15. Forsberg, K. J. et al. The shared antibiotic resistome of soil bacteria and human pathogens. *Science* **337**, 1107–1111 (2012).
16. Jiang, X. et al. Dissemination of antibiotic resistance genes from antibiotic producers to pathogens. *Nat. Commun.* **8**, 15784 (2017).
17. Medema, M. H. & Fischbach, M. A. Computational approaches to natural product discovery. *Nat. Chem. Biol.* **11**, 639–648 (2015).
18. Tang, X. et al. Identification of thiotetronic acid antibiotic biosynthetic pathways by target-directed genome mining. *ACS Chem. Biol.* **10**, 2841–2849 (2015).
19. Medema, M. H. et al. antiSMASH: rapid identification, annotation and analysis of secondary metabolite biosynthesis gene clusters in bacterial and fungal genome sequences. *Nucleic Acids Res.* **39**, W339–W346 (2011).
20. Asano, Y. & Lübbehüsen, T. L. Enzymes acting on peptides containing D-amino acid. *J. Biosci. Bioeng.* **89**, 295–306 (2000).
21. Allen, H. K., Moe, L. A., Rodbumrer, J., Gaarder, A. & Handelsman, J. Functional metagenomics reveals diverse β-lactamases in a remote Alaskan soil. *ISME J.* **3**, 243–251 (2009).
22. Reimer, D., Pos, K. M., Thines, M., Grün, P. & Bode, H. B. A natural prodrug activation mechanism in nonribosomal peptide synthesis. *Nat. Chem. Biol.* **7**, 888–890 (2011).
23. Reimer, D. & Bode, H. B. A natural prodrug activation mechanism in the biosynthesis of nonribosomal peptides. *Nat. Prod. Rep.* **31**, 154–159 (2014).
24. Brotherton, C. A. & Balskus, E. P. A prodrug resistance mechanism is involved in colibactin biosynthesis and cytotoxicity. *J. Am. Chem. Soc.* **135**, 3359–3362 (2013).
25. Lohans, C. T. et al. Biochemical, structural, and genetic characterization of tridecaptin A_1, an antagonist of *Campylobacter jejuni*. *ChemBioChem* **15**, 243–249 (2014).
26. Cochrane, S. A., Lohans, C. T., van Belkum, M. J., Bels, M. A. & Vederas, J. C. Studies on tridecaptin B_1, a lipopeptide with activity against multidrug resistant Gram-negative bacteria. *Org. Biomol. Chem.* **13**, 6073–6081 (2015).
27. Barsby, T., Kelly, M. T., Gagné, S. M. & Andersen, R. J. Bogorol A produced in culture by a marine *Bacillus* sp. reveals a novel template for cationic peptide antibiotics. *Org. Lett.* **3**, 437–440 (2001).
28. Yang, X., Huang, E., Yuan, C., Zhang, L. & Yousef, A. E. Isolation and structural elucidation of brevibacillin, an antimicrobial lipopeptide from *Brevibacillus laterosporus* that combats drug-resistant Gram-positive bacteria. *Appl. Environ. Microbiol.* **82**, 2763–2772 (2016).
29. Rawlings, N. D., Barrett, A. J. & Finn, R. Twenty years of the MEROPS database of proteolytic enzymes, their substrates and inhibitors. *Nucleic Acids Res.* **44**, D343–D350 (2016).
30. de la Fuente-Núñez, C., Mertens, J., Smit, J. & Hancock, R. E. The bacterial surface layer provides protection against antimicrobial peptides. *Appl. Environ. Microbiol.* **78**, 5452–5456 (2012).
31. Jiang, W., Bikard, D., Cox, D., Zhang, F. & Marraffini, L. A. RNA-guided editing of bacterial genomes using CRISPR-Cas systems. *Nat. Biotechnol.* **31**, 233–239 (2013).
32. Altenbuchner, J. Editing of the *Bacillus subtilis* genome by the CRISPR-Cas9 system. *Appl. Environ. Microbiol.* **82**, 5421–5427 (2016).
33. Breukink, E. & de Kruijff, B. Lipid II as a target for antibiotics. *Nat. Rev. Drug Discov.* **5**, 321–323 (2006).
34. Wencewicz, T. A. New antibiotics from Nature's chemical inventory. *Bioorg. Med. Chem.* **24**, 6227–6252 (2016).
35. Moffitt, M. C. & Neilan, B. A. Characterization of the nodularin synthetase gene cluster and proposed theory of the evolution of cyanobacterial hepatotoxins. *Appl. Environ. Microbiol.* **70**, 6353–6362 (2004).

Acknowledgements

This work was generously supported by a grant from the China Ocean Mineral Resources Research and Development Association (COMRRDA17SC01 to P.-Y.Q.). We thank J. Sun and A. Cheung for comments on the manuscript and Y.C. Yan for help with scripts development.

Author contributions

Y.-X.L., Z.Z., P.H., and W.-P.Z. performed bioinformatics analysis and chemical and biochemical experiments. All authors analyzed and discussed the results. P.-Y. Q. and Y.-X.L. designed the study and prepared the manuscript.

Competing interests

The authors declare no competing interests.

Additional information

Supplementary information is availble for this paper at https://doi.org/10.1038/s41589-018-0009-4.

Reprints and permissions information is available at www.nature.com/reprints.

Correspondence and requests for materials should be addressed to P.-Y.Q.

Publisher's note: Springer Nature remains neutral with regard to jurisdictional claims in published maps and institutional affiliations.

Methods

Statistical analyses. No statistical method was used to predetermine the sample size. The experiments were not randomized, and the investigators were not blinded to allocation during experiments and outcome assessment. Statistical significance of co-occurrences was determined by two Fisher's exact test (both two-sided), while significance of association between BogQ-like peptidase with NRPS was determined by Mann–Whitney U test (two-sided). For co-occurrences with phylogenetic corrections, phylogenetic generalized linear mixed model (PGLMM) was implemented. All statistics were calculated in R.

Bacteria strains, plasmids, oligonucleotides and general materials. Bacterial strains and plasmids used in this study are shown in Supplementary Tables 3 and 4. Oligonucleotide primers were synthesized by GenScript. Plasmid DNA was extracted with a TIANprep Mini Plasmid Kit from Tiangen. Gel extraction of DNA fragments and purification of ligation products were performed using a universal DNA Purification Kit from Tiangen. DNA sequencing was performed by BGI. Protino Ni-NTA Agarose was purchased from MACHEREY-NAGEL. SDS–PAGE gels were purchased from GenScript. Protein concentrations were determined by Quick Start Bradford Protein Assay from Bio-Rad. Optical densities of *E. coli* cultures were measured with a Thermo Scientific GENESYS 10 UV–Vis spectrophotometer at a wavelength of 600 nm. All bacterial strains used in the present study were routinely grown on a solid LB (pH 7.0) medium at 37 °C and in a liquid selected medium at 37 °C on a rotary shaker operated at 180 r.p.m. Minimum inhibitory concentration (MIC) determinations were performed in LB. For plasmid maintenance in *E. coli*, ampicillin (100 μg mL^{-1}) or kanamycin (50 μg mL^{-1}) was used. *B. subtilis* recombinants were selected on LB medium containing spectinomycin (100 μg mL^{-1}).

Computational analysis of biosynthesis gene clusters (BGCs). A total of 5,585 complete bacterial genomes (with a cut-off date of 20 October 2016) were retrieved from the NCBI Genome and subjected to BGC analysis using the standalone version of antiSMASH v3.0.5 (refs.[19,36]). To save time, only one additional annotation was performed, namely, smCOG analysis for the functional prediction and phylogenetic analysis of genes, whereas other analyses such as Blast comparison were not conducted. In total, 26,344 BGCs, including 6,879 NRP BGCs, were identified from complete bacterial genomes spanning the entire domain of bacteria. To investigate the associations between BogQ-like proteins and DNRP BGCs at the genome level, we performed a BGC analysis of 1,503 genomes (complete and draft) of the genera *Bacillus*, *Brevibacillus*, and *Paenibacillus*. The full list of genomes used in the present study is given in the Supplementary Dataset 1. In total, 403 BogQ-like proteins were harbored by 296 genomes of selected genera.

Pattern-based global genome mining. To gain insight into the biosynthesis capacity of bacterial natural products and their diverse biosynthesis logics, we created a series of scripts to collect information for all BGCs from the antiSMASH-annotated files, generating a large pattern matrix based on the presence or absence of the biosynthesis elements of all BGCs. The extracted biosynthesis information in the matrix contained 301 biosynthesis protein orthologs grouped by smCOG analysis, 40 NRPS/PKS domains, and 37 monomers. Amino acid monomers of NRPs, as determined by the substrate specificity of the adenylation (A) domains predicted by Minowa prediction algorithms, were further distinguished into D/L-aa based on the presence/absence of an epimerization domain (E) or a dual-functional condensation domain (C_{dual}) in the same module[2,5]. The potential of impact of bias issues related to A domains prediction algorithm on genome mining could not be excluded. BGCs encoding DNRPs were confirmed by the presence of an epimerase domain or a dual-functional domain in NRPS modules. As this approach does not appear to be applicable to nonmodular standalone adenylation enzymes, only modular A domains with other adjacent domains in the same module were selected in the present study. To globally target the BGCs of specific biosynthesis elements following biosynthesis logic, pattern searching was performed in the matrix. For instance, to target BGCs following the D-Asn specific activation mechanism, we searched for BGCs with the presence of both a D-Asn1 monomer incorporated by a typical C_s-Asn1-T-E starting module and E5 (ref. [23]). To target BGCs following the putative D-Orn/D-Trp specific inactivation mechanism, we searched for BGCs with both the D-Orn/D-Trp monomer and E5 present. By applying this approach to 1,503 genomes of the genera *Bacillus*, *Brevibacillus* and *Paenibacillus*, we targeted the bacteria strains harboring bogorol or tridecaptin BGCs (Supplementary Fig. 9).

Phylogenetic analyses. The phylogenetic tree of bacteria was built by PhyloPhlAn[37] using complete genomes for each species of bacteria and visualized by the interactive tree of life (iTOL)[38]. To obtain the phylogenetic tree of presumed D-aa-correlating peptidases, multiple sequence alignment was performed with 59 selected D-aa-correlated putative peptidase sequences using ClustalW, and this alignment was then employed to generate a phylogenetic tree based on maximum likelihood clustering by Mega7 (ref. [39]). A protein domain architecture data set was exported from HHMER[40]. The resulting phylogenetic tree was visualized using iTOL online tool. BogQ-like peptidases were identified by BLASTP and domain architecture searches in the NCBI database using the protein sequence of BogQ (WP_018673858.1) from *B. laterosporus* DSM 25 (ARFS00000000.1) as a query. The phylogenetic tree of BogQ-like peptidases was built by Mega7. Amino acid sequences for the species and their accession numbers are given in the Supplementary Dataset 4.

Co-occurrence networks. By applying network analysis tools widely used to explore interactions and associations between entities, we could assess the co-occurrence patterns of biosynthesis elements to investigate the biosynthesis logic of natural products. A co-occurrence network between the D-aa monomers and BGC-associated resistance determinants was built based on the observed co-occurrences between D-aa monomers of DNRPs and the selected orthologs for putative antibiotic resistance determinants (49 enzymes, 30 transporters, and 32 regulators) in 6,879 NRPS BGCs. The antibiotic resistance determinants were manually selected based on the Comprehensive Antibiotic Resistance Database[41] (for the full list of biosynthesis elements and selected resistance determinants, see the Supplementary Dataset 2). To ensure that the associations observed here were not random and to minimize false-positive predictions, we restricted our analysis to co-occurrence in at least 10% of D-aa ($\frac{A \cap B}{A} > 10\%$), and all observed co-occurrences were tested through two pairwise comparisons. The first step was to evaluate the statistical significance (P_1) of the co-occurrence between D-aa monomers and the associated resistance elements via pairwise comparison of NRPs with D-aa (D) vs. NRPs without D-aa (ND). The second step was to determine the significance (P_2) of D-stereospecific co-occurrence (P_2) via pairwise comparison of NRPs with D-aa (D) vs. NRPs without D-aa, but with their L enantiomers (L). The co-occurrences were tested using the two-sided Fisher's exact test, with the *P* value further adjusted using the Benjamini–Hochberg correction. (Supplementary Data Set 3) The *n* value for P_1 was 6,879, whereas that for P_2 varied with monomers (Abu: 3; Ahp: 14; Ala: 964; Alaninol: 247; Arg: 344; Asn: 418; Asn1: 111; Asp: 581; Bht: 32; Cys: 1119; Dab: 391; Gln: 335; Glu: 476; Gly: 1094; His: 24; Hpg: 127; Ile: 256; Leu: 932; Lys: 770; Orn: 822; Phe: 437; Pro: 371; Ser: 2559; Thr: 1424; Trp: 506; Tyr: 335; Val: 1149). A significant co-occurrence was defined as one with $P_1 < 0.005$, $P_2 < 0.05$, RR (Risk ratio)$_1 > 1.5$, and $RR_2 > 1.5$. The entire co-occurrence network was visualized by Gephi[42]. The significant co-occurrence between D-aa and E5 was further tested after systematically correcting for phylogenetic relatedness using the phylogenetic generalized linear mixed model (PGLMM) for binary data in the 'ape' package in R[43–45].

Metabolic analysis by UPLC-MS. For UPLC–ESI–MS analysis, all samples dissolved in 100 mL of MeOH were analyzed by the Waters ACQUITY UPLC system (Waters ACQUITY, USA) coupled with a Bruker microTOF-q II mass spectrometer (Bruker Daltonics GmbH, Bremen, Germany). A 2-μL aliquot of each sample was injected into a Waters BEH C18 reversed-phase UPLC column (1.7 μm, 150 mm × 2.1 mm inner diameter) and washed by a gradient elution (A, CH_3CN with 0.1% formic acid (FA); B, H_2O with 0.1% FA; gradient: 5% A over 2 min, 5–100% A from 2 to 22 min, 100% A from 22 to 25 min, and 100–5% A from 25 to 27 min; flow rate, 0.25 mL/min). TOF–MS settings during the UPLC gradient were as follows: acquisition, mass range *m*/*z* 200–2,000 Da; source, gas temperature 200 °C, gas flow 8 L/min; nebulizer 4 bar, ion polarity positive; scan source parameters, capillary exit 140 V, skimmer 50 V. MS data was acquired with HyStar chromatography software (Bruker Daltonik) and processed with Bruker Compass DataAnalysis 4.0 software (Bruker Daltonik). High-resolution (HR)–ESI–MS spectra were recorded on a Bruker microTOF II ESI–TOF–MS spectrometer.

Isolation of compounds bogorols and tridecaptins. In the genera of *Brevibacillus* and *Paenibacillus*, three strains with complete genomes that harbor DNRP BGCs and the putative corresponding DRP genes, as well as another seven strains with draft genome data that harbor similar BGCs were purchased from bacterial collection centers. The selected strains were cultivated in 5 mL of a modified tryptic soy broth medium (MTSB, 30 g/L tryptic soy broth (Sigma), 20.0 g/L starch, 2.0 g/L $MgSO_4{\cdot}7H_2O$, 10.0 g/L $CaCO_3$) and then incubated at 30 °C or 37 °C on a shaker (250 r.p.m.). After 12–48 h of incubation, each culture supernatant was extracted with Diaion HP-20 (0.5 g; Sigma–Aldrich) and eluted with 20% isopropyl alcohol (IPA, 4.0 mL) and 80% IPA with 0.1% trifluoroacetic acid (TFA; 0.50 mL). The second partition collected was evaporated to dryness using a vacuum concentrator. Each extract prepared was re-dissolved in 100 μL of MeOH and centrifuged at 15,000 r.p.m. for 10 min before UPLC–MS analysis as described above. Metabolic analysis of the selected strains, led to the identification of *B. laterosporus* DSM 25, ATCC 9141 and *P. polymyxa* CICC 10580 that produced DNRPs and their putative truncated products.

P. polymyxa CICC10580 was cultivated in two 2.5 L flasks containing 1.0 L of a glucose starch calcium carbonate (GSC) medium (20 g/L glucose, 20 g/L starch, 20 g/L $(NH_4)_2SO_4$, 10 g/L yeast extract, 2.6 g/L K_2HPO_4, 0.1 g/L $FeSO_4{\cdot}7H_2O$, 0.5 g/L$MgSO_4{\cdot}7H_2O$, 0.25 g/L NaCl, 9.0 g/L $CaCO_3$) at 30 °C for tridecaptin B production. The culture supernatant was extracted with Diaion HP-20 (50 g; Sigma-Aldrich) and eluted with 20% IPA (2.0 L), 40% IPA (2.0 L) and 80% IPA with 0.1% trifluoroacetic acid (TFA; 1.0 L). The third partition collected was evaporated to dryness using a vacuum concentrator and then separated by a semipreparative RP-HPLC column (Waters 600 apparatus using a semi-preparative

C-18 Phenomenex Luna 5 µm (10 mm × 250 mm) and monitored by a UV detector (Waters 2475)) with 40% MeCN in water to yield tridecaptin B (**1**,**2**).

B. laterosporus DSM 25 was cultivated in two 2.5 L flasks containing 1.0 L of a modified tryptic soy broth medium at 30 °C for 2 d for bogorol production. The culture supernatant was extracted with Diaion HP-20 (50 g; Sigma-Aldrich) and eluted with 20% IPA (2.0 l), 40% IPA (0.5 l), 60% IPA (0.5 l), and 80% IPA with 0.1% trifluoroacetic acid (0.5 L). All partitions were evaporated to dryness using a vacuum concentrator and dissolved in methanol for HPLC purification. The 40% IPA partition was then separated by the semipreparative RP-HPLC column with 30% MeCN in water to yield truncated bogorol analogs (**9**,**10**) at 12–26 mg L^{-1}. The 80% IPA partition was separated by the semipreparative RP-HPLC column with a gradient of 35–55% MeCN in water with 0.1% trifluoroacetic acid to yield mixture of bogorol A,B (**3**,**4**) at 1.6 mg L^{-1}. As *B. laterosporus* ATCC 9141 produced a higher yield of bogorols based on UPLC–MS analysis results, bogorols were extracted from *B. laterosporus* ATCC 9141 cultured in 2.0 L of a MTSB medium at 30 °C for 2 d following the same extraction and partition methods described above. The 80% IPA partition was subjected to open C-18 column and eluted with 60% MeOH (200 mL), 80% MeOH (200 mL), 100% MeOH (200 mL), and 100% MeOH with 0.1% trifluoroacetic acid (200 mL). The partition of 100% MeOH with 0.1% trifluoroacetic acid was subjected to UPLC–MS analysis and identified to be total bogorol fraction. The Bs (Bs: total bogorols extraction from *B. laterosporus* ATCC 9141) was further separated by semipreparative RP-HPLC column with a gradient of 30–50% MeCN in water with 0.1% trifluoroacetic acid to yield pure bogorols A–E (**3**–**8**).

Structure elucidation. ^{1}H, ^{1}H-^{1}H-COSY, ^{1}H-^{13}C-HSQC, and ^{1}H-^{13}C-HMBC NMR spectra for compounds **9** and **10** were recorded on a Bruker AV500 spectrometer (500 MHz) using MeOH-d_4 (^{1}H-NMR MeOH-d_4: δ_H = 3.31 p.p.m.; MeOH-d_4: δ_C = 49.00 p.p.m.). Amino acid configurations of **3**, **9**, and **10** were determined using the advanced Marfey's method[46]. The purified compounds **3**, **9**, and **10** (0.1–0.2 mg) were hydrolyzed in 6 M HCl at 120 °C overnight. Each solution was evaporated to dryness under a stream of dry N_2, and the residue was dissolved in 100 µL water and divided into two portions. Each portion was treated with 20 µL of $NaHCO_3$ (1 M) and 50 µL of 1-fluoro-2, 4-dinitrophenyl-5-L-leucinamide (L-FDLA) or D-FDLA (1 M) at 40 °C for 2 h. The reaction was quenched with 5 µL HCl (1 M) and diluted with 200 µL of MeOH. The stereochemistry was determined by comparison of the L-/D FDLA derivatized samples using UPLC–MS analysis.

Heterologous expression and *in vivo* cleavage assay of BogQ and TriF. The gene *bogQ* was PCR amplified from the genomic DNA of *B. laterosporus* DSM 25 and ATCC 9141 using the primers BogQ-B-NheI-F/BogQ-B-SphI-R and BogQ-9141-B-NheI-F/BogQ9141-B-SphI-R. The resultant products were digested and cloned into NheI and SphI sites of pDR111 (ref.[47]), generating pDR111-*bogQ* and pDR111-9141-*bogQ*, respectively. The *triF* gene was PCR amplified from the genomic DNA of *P. polymyxa* CICC 10580 using the primers TriF-B-SalI-F and TriF-B-SphI-R. The resulting product was digested and cloned into SalI and SphI sites of pDR111, generating pDR111-*triF*. The purified plasmids pDR111-*bogQ*, pDR111-9141-*bogQ* and pDR111-*triF* from an amp^{R} clone of *E. coli* was then transformed into *B. subtilis* via natural competence transformation for in vivo cleavage assay of BogQ and TriF. *B. subtilis* 168/pDR111-*bogQ*, *B. subtilis* 168/pDR111-9141-*bogQ*, *B. subtilis* 168/pDR111-*triF* and *B. subtilis* 168/pDR111 (as the control) were cultivated in duplicate in a 2 mL LB medium supplemented with spectinomycin (100 µg mL^{-1}) in a 15 mL Falcon tube at 30 °C with shaking on a rotary shaker operated at 180 r.p.m. The experiments were started with inoculation of 2 mL of 4 h-old pre-culture (OD_{600} = 0.2–0.4) and administration of 0.04 mg of compounds **1** and **3** dissolved in DMSO. 1-mL samples were taken at 12 h and extracted with 1 mL of EtOAc. The organic layer was evaporated to dryness and re-dissolved in 50 µL of MeOH for analysis by UPLC–ESI–MS.

Cloning, overexpression, and purification of BogQ, TriF$_{pep}$ and their variants. The genes for BogQ, bogQ$_{pep}$, and their variants were PCR amplified from *B. laterosporus* DSM 25, ATCC 9141, while the genes for TriF, TriF$_{pep}$, and their variants were PCR amplified from *P. polymyxa* CICC 10580 genomic DNA using the primer shown in Supplementary Table 4. Sequences encoding the signal peptide were removed to facilitate cytoplasmic expression and protein purification. TriF$_{pep}$ is the soluble periplasmic peptidase domain (residues 32–500) without the signal peptide or the four hydrophobic transmembrane helices. BogQ is the full-length sequence of the peptidase without signal peptide, whereas BogQ$_{pep}$ is the soluble periplasmic peptidase domain (residues 36–470) without the sequences for the signal peptide or three S-layer homologous domains. Amplified fragments and expression vectors were digested with the appropriate restriction enzymes (New England BioLabs) shown in Supplementary Table 4, and then ligated into linearized expression vectors using the Quick Ligation Kit (New England BioLabs). The ligated constructs were then electrotransformed into competent *E. coli* BL21 for recombinant protein expression and stored at −80 °C as frozen LB/glycerol stocks. *BogQ*, *bogQ$_{pep}$*, *triF*, and their variants were ligated into the pET-28a vector to encode N- and C-terminal His6-tagged constructs, whereas *triF$_{pep}$* and its variants were ligated into the pET-24a vector to encode C-terminal His6-tagged constructs.

The recombinant strain *E. coli* BL21 carrying pET-28a-*bogQ* was cultured overnight at 37 °C in LB medium in the presence of 50 µg/mL kanamycin. 6 mL of the overnight culture was diluted 1:100 into 600 mL of LB medium containing 50 µg/mL kanamycin and incubated at 37 °C until an OD_{600} = 0.5–0.6 was reached. The culture was incubated at 15 °C for 30 min, and isopropyl β-D-1-thiogalactopyranoside (IPTG) was added to a final concentration of 187 µM to induce BogQ expression. After incubating at 15 °C overnight with shaking at 150 r.p.m., the cells were harvested by centrifugation (4,000 r.p.m. for 20 min at 4 °C) and resuspended in a lysis buffer containing 50 mM NaH_2PO_4, 300 mM NaCl, 10 mM imidazole and lysed by sonication. The lysate was clarified by centrifugation (10,000 r.p.m. for 40 min at 4 °C). The supernatant was incubated with 0.8 mL of Ni-NTA resin for 4 h at 4 °C. The mixture was centrifuged (2,000 r.p.m. for 3 min) and the unbound fraction discarded. The Ni-NTA was resuspended in 10 mL of wash buffer (50 mM NaH_2PO_4, 300 mM NaCl, and 50 mM imidazole, pH 8), and loaded into a column under gravity flow. The mixture was then washed four times with 10 mL washing buffer. The protein was eluted three times with 1 mL elution buffer (50 mM NaH_2PO_4, 300 mM NaCl, and 250 mM imidazole), collected in three tubes and analyzed by SDS–PAGE to ascertain the presence and purity of proteins. Fractions containing the desired protein were dialyzed twice against 2 L of storage buffer (20 mM Tris–HCl, 50 mM NaCl, 10% (v/v) glycerol, pH 8). BogQ$_{pep}$ and BogQ mutants were purified under the same conditions mentioned above.

The recombinant strain pET-24a-*tirF$_{pep}$ E. coli* BL21 was cultured overnight at 37 °C in an LB medium in the presence of 50 µg/mL kanamycin. 8 mL of the overnight culture was diluted 1:100 into 800 mL of LB medium containing 50 µg/mL kanamycin and incubated at 37 °C until OD_{600} = 0.5–0.6 was reached. The culture was incubated at 15 °C for 30 min, and IPTG was added to a final concentration of 500 µM to induce TriF$_{pep}$ expression. After incubating at 15 °C overnight with shaking at 150 r.p.m., the cells were harvested by centrifugation (4,000 r.p.m. for 20 min at 4 °C) and resuspended in lysis buffer containing 50 mM NaH_2PO_4, 300 mM NaCl, and 10 mM imidazole and lysed by sonication. The lysate was clarified by centrifugation (10,000 r.p.m. for 40 min at 4 °C). The supernatant was incubated with 1.0 mL of Ni-NTA resin for 4 h at 4 °C. The mixture was centrifuged (2,000 r.p.m. for 3 min) and the unbound fraction discarded. The Ni-NTA was resuspended in 10 mL of wash buffer (50 mM NaH_2PO_4, 300 mM NaCl, 50 mM imidazole, pH 8) and loaded into a column under gravity flow. The mixture was then washed four times with 10 mL wash buffer. The protein was eluted three times with 1 mL of elution buffer (50 mM NaH_2PO_4, 300 mM NaCl, and 250 mM imidazole), collected in three tubes and analyzed by SDS–PAGE to ascertain the presence and purity of proteins. Fractions containing the desired protein were dialyzed twice against 2 L of storage buffer (20 mM Tris–HCl, 50 mM NaCl, 10% (v/v) glycerol, pH 8). TriF$_{pep}$ protein was ultimately concentrated to ~35 mg/mL by Amicon Ultra centrifugal filters (Millipore) and stored as stock at −20 °C. TriF$_{pep}$ mutants were purified with the same conditions mentioned above.

Biochemical characterization of BogQ, TriF$_{pep}$ and their variants. The predicted catalytic functions of BogQ, TriF$_{pep}$, and their variants were confirmed with UPLC–MS analysis of enzyme reactions. The assay mixture (total volume 30 µL in 25% phosphate-buffered saline (PBS) buffer, pH 7.4), which contain purified proteins (final concentration: BogQ or its variants, 2.0 µM; TriF$_{pep}$ or its variants, 2.0 µM), and in DMSO dissolved tridecaptins, bogorols or synthetic analogs (final concentrations: 20–200 µM), was incubated for 15 s–24 h at 37 °C. Three volumes of cold methanol (90 µL) was added to samples, which were then incubated at −80 °C for 1 h to precipitate protein. The samples were centrifuged at 15,000 r.p.m. for 10 min, and the supernatant (2 µL) was injected into the same UPLC–MS system described above. The relative cleavage efficiency of enzymes for test compounds was determined from UPLC–MS-extracted ion chromatogram traces: the remaining peak area of a digested derivative (AIC_{sample}) was divided by the peak area obtained from a control sample incubated under the same conditions but in the absence of test proteins ($AIC_{control}$) to obtain cleavage ratios ($1 - (AIC_{sample}/AIC_{control})$).Note that a cleavage ratio value of 0.00 corresponds to that not corresponding hydrolytic fragment was detected. Each assay was independently performed in triplicate.

Kinetic analysis of BogQ. To determine the kinetics of BogQ, the assays were performed at the 40 µL scale with 100 nM BogQ and an 1.56–400 µ M substrate (**3** and **46**) in 25% phosphate-buffered saline (PBS, pH 7.4) at 37 °C for 100 s. The reactions were quenched by adding 160 µL methanol. After centrifugation, the supernatant was analyzed by UPLC–MS as mentioned above. Velocities were calculated and plotted as a function of substrate concentrations. This allowed the determination of K_M and k_{cat} by nonlinear regression with OriginPro 8.0 software using the Michaelis-Menten equation: $v = V_{max} \times S/(K_M + S)$. where v is the reaction velocity, S is the substrate concentration. K_M and k_{cat} values represent mean ± s.d. of three independent replicates.

Gene deletion using the CRISPR–Cas9 system. Vector pJOE8999-*bogQ* was constructed to delete 1.8 kb of gene *bogQ* in chromosomes using the CRISPR–Cas9 system[32]. With the help of the sgRNA Designer tool provided by the Broad Institute[48], candidate sgRNA sequences were identified and chosen for

oligonucleotide synthesis. In the first step, the plasmid pJOE8999 was cut with BsaI and the *lacZ* α fragment was replaced by the two complementary oligonucleotides BogQ-41-sgRNA-F/R. In the second step, two fragments flanking *bogQ* with lengths of about 400 bp were amplified by PCR using primers BQ-41-Up-F/R and BQ-41-Do-F/R from *B. laterosporus* ATCC 9141 chromosomal DNA as the template and then cut with SfiI and inserted between the two SfiI sites to give pJOE8999-*bogQ* (Supplementary Fig. 16a).

Plasmid pJOE8999-*bogQ* was transformed into *B. laterosporus* ATCC 9141 according to the electroporation method. First, an overnight culture of *B. laterosporus* ATCC 9141 in a tryptic soy broth containing 0.5 mol/L D-sorbitol was diluted 20-fold in growth medium (a 50 mL LB containing 0.5 mol/L D-sorbitol) and incubated at 37 °C on a shaker until the cell density reached an OD_{600} of 0.80–1.0. The cultures were collected and cooled with ice water for 10 min, and the cells were harvested by centrifugation at 4,000 *g* for 10 min at 4 °C. After washing the cells four times with an ice-cooled electroporation buffer (250 mmol/L sucrose, 1 mmol/L $MgCl_2$, 1 mmol/L HEPES, and 10% glycerol), the competent cells were resuspended in electroporation buffer at a concentration of about 2.0×10^{10} cfu/mL. These competent cells were mixed with 100–500 ng of the pJOE8999-*bogQ* vector DNA, transferred to 1 mm cuvettes, and placed on ice for at least 10 min. The sample was pulsed using a Gene Pulser with a voltage of 16 kV cm^{-1}, a capacitance of 25 mF, and a resistance of 200 Ω. The cell suspension was then immediately mixed with 1 mL of recovery medium (LB containing 0.5 mol/L D-sorbitol), incubated at 30 °C for 3 h, and plated on the selective LB agar plates containing 25 g ml L^{-1} kanamycin and 0.2% mannose for induction of *cas9*. After incubation at 30 °C for 2 d, kanamycin-resistant transformants were confirmed by colony PCR of the *cas9* gene. The positive colonies with knockout vector were streaked onto LB plates without antibiotics and incubated at 50 °C for plasmid curing. On the next day, these colonies were streaked on LB plates to obtain single colonies at 42 °C. The colonies cured of plasmid were confirmed by streaking them onto LB plates containing kanamycin (25 mg/L); colonies cured of plasmid failed to grow at 37 °C. The plasmid-cured cells were confirmed by colony PCR using the outer primers from the homology templates. In the case of a successful deletion, the fragment size would be reduced from 2.6 kb to 0.8 kb (Supplementary Fig. 16a).

Antibacterial assays. *B. laterosporus* DSM 25, ATCC 9141, ATCC 9141/Δ*BogQ*, *S. aureus* ATCC 43300, UST950701-005, *B. subtilis* 168, *E. coli* Top10 and *P. aeruginosa* PAO1 were grown at 30 °C with continuous shaking overnight in LB medium. Overnight-grown bacteria were grown to early stationary phase and adjusted in LB to 5.0×10^5 cfu/mL in 96-well microtiter plates, mixed with varying concentrations (2048, 1024, 512, 256, 128, 64, 32, 16, 8, 4, 2, 1, 0.5, 0.25 and 0.125 μg mL^{-1}) of test compounds and incubated at 30 °C for 24 h. Cell growth was evaluated by measuring the optical density at 595 nm (Thermo Scientific Multiskan FC multiplate photometer; Waltham, MA, USA), and the lowest compound concentrations, which displayed no bacterial growth, were defined as the MIC.

The antibiotics inactivation assay of BogQ was performed using a Kirby–Bauer assay, 100 μL of a PBS buffer containing bogorol (2.5 mg mL^{-1}), bacitracin (10 mg mL^{-1}), enduracidin (0.50 mg mL^{-1}) or ramoplanin (0.50 mg mL^{-1}) was inoculated with or without 2.0 μM BogQ and incubated at 37 °C for 12 h. 5 μL of each reaction product was dropped onto filter paper and dried. The indicator strain *B. subtilis* 168 or *S. aureus* ATCC 43300 was swabbed uniformly across a culture plate. A filter-paper disk, impregnated with the compound to be tested, is then placed on the surface of the agar and cultured at 37 °C for 24 h.

Homology-based BogQ protein models. Electrostatic fields around the surface of enzymes play a crucial role in molecular recognition because of the attractive or repulsive effect of the coulombic potential[49]. We therefore calculated the electrostatic potential molecular surface of BogQ enzymes based on protein structure homology modeling. For SWISS-MODEL[50] calculation, the closely related D-Asn1-specific activation peptidase ClbP (PDB entry 4E6X) from *E. coli* was selected as an appropriate template with a known three-dimensional structure. The PDB2PQR program[51] (version 2.0.0.) was used to calculate the electrostatic surface potential map of protein models, which were visualized with the Chimera program. On the side harboring a catalytic groove, we observed in BogQ a putative strong negative electrostatic potential surface restricted to the catalytic groove.

Substrate synthesis and characterization data. Using **3** as the starting material, we synthesized the corresponding tri-Boc-bogorol A (**45**) via a standard Boc protection procedure. Di-*tert*-butyl dicarbonate (2.0 equivalent) was added to a solution of **3** (2 mM) and $NaHCO_3$ (0.1 M) in methanol (0.2 mL). The mixture was shaken at 150 r.p.m. for 2 h at 25 °C, and the resultant reaction mixture was further purified by HPLC.

Synthetic peptides (**22**–**44**, **17**, and **18**) were purchased through the custom peptide synthesis service of GenScript Biotech Corporation. Solid-phase peptide synthesis was performed according to standard Fmoc SPPS methods. Peptides were assembled on a Wang resin and isolated using the solid-phase extraction method[52]. Peptides from GenScript were delivered as lyophilized materials that had been purified by HPLC. All purified peptides were examined by HPLC–MS (electrospray ionization; ESI). Peptides purified by HPLC to a purity of >90% were used for in vitro assay. All pure peptides were dissolved in DMSO at 32 mg mL^{-1} as stock solutions and stored at −20 °C. For compound characterization see the Supplementary Note.

Code availability. Source code for BGC analysis and networking analysis will be made available upon reasonable request.

Life Sciences Reporting Summary. Further information on experimental design is available in the Life Sciences Reporting Summary.

Data availability. All data sets generated or analyzed in the current study are included in this published article (and its Supplementary information) or are available from the corresponding author upon reasonable request. The biosynthesis gene cluster for bogorol has been deposited in GenBank under accession number KY810814.

References

36. Weber, T. et al. antiSMASH 3.0-a comprehensive resource for the genome mining of biosynthetic gene clusters. *Nucleic Acids Res.* **43**, W237–W243 (2015).
37. Segata, N., Börnigen, D., Morgan, X. C. & Huttenhower, C. PhyloPhlAn is a new method for improved phylogenetic and taxonomic placement of microbes. *Nat. Commun.* **4**, 2304 (2013).
38. Letunic, I. & Bork, P. Interactive tree of life (iTOL)v3: an online tool for the display and annotation of phylogenetic and other trees. *Nucleic Acids Res.* **44**, W242–W245 (2016).
39. Kumar, S., Stecher, G. & Tamura, K. MEGA7: molecular evolutionary genetics analysis version 7.0 for bigger datasets. *Mol. Biol. Evol.* **33**, 1870–1874 (2016).
40. Finn, R. D. et al. HMMER web server: 2015 update. *Nucleic Acids Res.* **43**, W30–W38 (2015).
41. McArthur, A. G. et al. The comprehensive antibiotic resistance database. *Antimicrob. Agents Chemother.* **57**, 3348–3357 (2013).
42. Bastian, M., Heymann, S. & Jacomy, M. Gephi: an open source software for exploring and manipulating networks. *Proc. Int. AAAI Conf. Weblogs Soc. Media* (Association for the Advancement of Artificial Intelligence, 2009).
43. Ives, A. R. & Matthew, R. H. Generalized linear mixed models for phylogenetic analyses of community structure. *Ecol. Monogr.* **81**, 511–525 (2011).
44. Ives, A. R. & Garland, T. Jr. Phylogenetic logistic regression for binary dependent variables. *Syst. Biol.* **59**, 9–26 (2010).
45. Miller, J. E. D., Anthony, R. I., Susan, P. H. & Ellen, I. D. Early- and late-flowering guilds respond differently to landscape spatial structure. *J. Ecol.* https://doi.org/10.1111/1365-2745.12849 (2017).
46. Fujii, K., Ikai, Y., Oka, H., Suzuki, M. & Harada, K. A nonempirical method using LC/MS for determination of the absolute configuration of constituent amino acids in a peptide: combination of Marfey's method with mass spectrometry and its practical application. *Anal. Chem.* **69**, 5146–5151 (1997).
47. Wagner, J. K., Marquis, K. A. & Rudner, D. Z. SirA enforces diploidy by inhibiting the replication initiator DnaA during spore formation in *Bacillus subtilis*. *Mol. Microbiol.* **73**, 963–974 (2009).
48. Doench, J. G. et al. Optimized sgRNA design to maximize activity and minimize off-target effects of CRISPR-Cas9. *Nat. Biotechnol.* **34**, 184–191 (2016).
49. Baker, N. A., Sept, D., Joseph, S., Holst, M. J. & McCammon, J. A. Electrostatics of nanosystems: application to microtubules and the ribosome. *Proc. Natl. Acad. Sci. USA* **98**, 10037–10041 (2001).
50. Guex, N. & Peitsch, M. C. SWISS-MODEL and the Swiss-PdbViewer: an environment for comparative protein modeling. *Electrophoresis* **18**, 2714–2723 (1997).
51. Dolinsky, T. J. et al. PDB2PQR: expanding and upgrading automated preparation of biomolecular structures for molecular simulations. *Nucleic Acids Res.* **35**, W522–W525 (2007).
52. Wang, S. S. *p*-alkoxybenzyl alcohol resin and *p*-alkoxybenzyloxycarbonylhydr azide resin for solid phase synthesis of protected peptide fragments. *J. Am. Chem. Soc.* **95**, 1328–1333 (1973).

nature research

Corresponding author(s): Pei-Yuan Qian

☐ Initial submission ☒ Revised version ☐ Final submission

Life Sciences Reporting Summary

Nature Research wishes to improve the reproducibility of the work that we publish. This form is intended for publication with all accepted life science papers and provides structure for consistency and transparency in reporting. Every life science submission will use this form; some list items might not apply to an individual manuscript, but all fields must be completed for clarity.

For further information on the points included in this form, see Reporting Life Sciences Research. For further information on Nature Research policies, including our data availability policy, see Authors & Referees and the Editorial Policy Checklist.

Experimental design

1. Sample size

Describe how sample size was determined.

Sample size for BGC analysis was chosen on the basic of online available bacterial complete genome in Genbank (cut-off date October 20, 2016).

2. Data exclusions

Describe any data exclusions.

no data were excluded

3. Replication

Describe whether the experimental findings were reliably reproduced.

All attempts at replication were successful

4. Randomization

Describe how samples/organisms/participants were allocated into experimental groups.

No randomization, not studies involving animals or human research participants

5. Blinding

Describe whether the investigators were blinded to group allocation during data collection and/or analysis.

No blinding, not studies involving animals or human research participants

Note: all studies involving animals and/or human research participants must disclose whether blinding and randomization were used.

6. Statistical parameters

For all figures and tables that use statistical methods, confirm that the following items are present in relevant figure legends (or in the Methods section if additional space is needed).

n/a	Confirmed
☐	☒ The exact sample size (*n*) for each experimental group/condition, given as a discrete number and unit of measurement (animals, litters, cultures, etc.)
☐	☒ A description of how samples were collected, noting whether measurements were taken from distinct samples or whether the same sample was measured repeatedly
☐	☒ A statement indicating how many times each experiment was replicated
☐	☒ The statistical test(s) used and whether they are one- or two-sided (note: only common tests should be described solely by name; more complex techniques should be described in the Methods section)
☐	☒ A description of any assumptions or corrections, such as an adjustment for multiple comparisons
☐	☒ The test results (e.g. *P* values) given as exact values whenever possible and with confidence intervals noted
☐	☒ A clear description of statistics including central tendency (e.g. median, mean) and variation (e.g. standard deviation, interquartile range)
☐	☒ Clearly defined error bars

See the web collection on statistics for biologists for further resources and guidance.

Software

Policy information about availability of computer code

7. Software

Describe the software used to analyze the data in this study.	OriginPro 8.0, standalone version of antiSMASH v3.0.5., Gephi, PhyloPhlAn, iTOL and Mega7

For manuscripts utilizing custom algorithms or software that are central to the paper but not yet described in the published literature, software must be made available to editors and reviewers upon request. We strongly encourage code deposition in a community repository (e.g. GitHub). *Nature Methods* guidance for providing algorithms and software for publication provides further information on this topic.

Materials and reagents

Policy information about availability of materials

8. Materials availability

Indicate whether there are restrictions on availability of unique materials or if these materials are only available for distribution by a for-profit company.	All bacterial strains generated for this study will be provided to other researchers upon request.

9. Antibodies

Describe the antibodies used and how they were validated for use in the system under study (i.e. assay and species).	No antibodies were used

10. Eukaryotic cell lines

a. State the source of each eukaryotic cell line used.	No eukaryotic cell lines were used
b. Describe the method of cell line authentication used.	No eukaryotic cell lines were used
c. Report whether the cell lines were tested for mycoplasma contamination.	No eukaryotic cell lines were used
d. If any of the cell lines used are listed in the database of commonly misidentified cell lines maintained by ICLAC, provide a scientific rationale for their use.	No eukaryotic cell lines were used

Animals and human research participants

Policy information about studies involving animals; when reporting animal research, follow the ARRIVE guidelines

11. Description of research animals

Provide details on animals and/or animal-derived materials used in the study.	No animals were used

Policy information about studies involving human research participants

12. Description of human research participants

Describe the covariate-relevant population characteristics of the human research participants.	don't involve human research participants